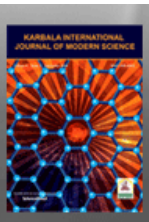

Karbala International Journal of Modern Science

Volume 9 | Issue 2 Article 5

Modifying Barium Hexaferrite Magnets by Adding Sol-Gel Synthesized Cobalt Ferrite Phase

Thanida Charoensuk
Thailand Center of Excellence in Physics, Ministry of Higher Education, Science, Research and Innovation, Bangkok, Thailand

Wannisa Thongsamrit
Thailand Center of Excellence in Physics, Ministry of Higher Education, Science, Research and Innovation, Bangkok, Thailand

Anuchit Hunyek
Program of General Education - Science (Physics), Faculty of Liberal Arts, Rajamangala University of Technology Rattanakosin, Wangkaikangwon Campus, Prachuap Khiri Khan, Thailand

Komkrich Chokprasombat
Department of Physics, Faculty of Science, Thaksin University, Phatthalung Campus, Thailand

Pongsakorn Jantaratana
Department of Physics, Faculty of Science, Kasetsart University, Chatuchak, Bangkok, Thailand

See next page for additional authors

Recommended Citation

Charoensuk, Thanida; Thongsamrit, Wannisa; Hunyek, Anuchit; Chokprasombat, Komkrich; Jantaratana, Pongsakorn; and Sirisathitkul, Chitnarong (2023) "Modifying Barium Hexaferrite Magnets by Adding Sol-Gel Synthesized Cobalt Ferrite Phase," *Karbala International Journal of Modern Science*: Vol. 9 : Iss. 2 , Article 5.
Available at: https://doi.org/10.33640/2405-609X.3292

Modifying Barium Hexaferrite Magnets by Adding Sol-Gel Synthesized Cobalt Ferrite Phase

Abstract

Combining various types of ferrites brings about magnetic properties desirable for different applications. This study aims to modify barium hexaferrite ($BaFe_{12}O_{19}$) by physically mixing it with cobalt ferrite ($CoFe_2O_4$). $BaFe_{12}O_{19}/CoFe_2O_4$ magnets were produced by ball-milling and pressing sol-gel-derived ferrite powders. The ferrite composites showed variations in magnetic properties from $BaFe_{12}O_{19}$ magnets with a saturation magnetization of 69.46 emu/g and a maximum energy product of 0.4529 MGOe. For the $BaFe_{12}O_{19}$:$CoFe_2O_4$ weight ratio of 4:1, both satura-tion and remanent magnetizations were increased due to the addition of $CoFe_2O_4$ with high magnetizations. However, the magnetizations were reduced when the BaFe12O19:CoFe2O4 ratio was reduced to 2:1. On the other hand, the coercivity was monotonously decreased with increasing $CoFe_2O_4$. Interestingly, the maximum energy product in this study was linearly decreased with the bulk density of the magnets from 3.59 to 3.15 g/cm_3. It is concluded that magnetic properties could be modified from a facile physical mixing of ferrites.

Keywords

Barium hexaferrite; Cobalt ferrite; Sol-gel reaction; Powder compaction; Nanocomposite magnet

Authors

Thanida Charoensuk, Wannisa Thongsamrit, Anuchit Hunyek, Komkrich Chokprasombat, Pongsakorn Jantaratana, and Chitnarong Sirisathitkul

RESEARCH PAPER

Modifying Barium Hexaferrite Magnets by Adding Sol−Gel Synthesized Cobalt Ferrite Phase

Thanida Charoensuk [a], Wannisa Thongsamrit [a,b], Anuchit Hunyek [c], Komkrich Chokprasombat [d], Pongsakorn Jantaratana [e], Chitnarong Sirisathitkul [f,g,*]

[a] Thailand Center of Excellence in Physics, Ministry of Higher Education, Science, Research and Innovation, Bangkok, Thailand
[b] Center of Excellence in Smart Materials Research and Innovation, King Mongkut's Institute of Technology Ladkrabang, Ladkrabang, Bangkok, Thailand
[c] Program of General Education - Science (Physics), Faculty of Liberal Arts, Rajamangala University of Technology Rattanakosin, Wangkaikangwon Campus, Prachuap Khiri Khan, Thailand
[d] Department of Physics, Faculty of Science, Thaksin University, Phatthalung Campus, Thailand
[e] Department of Physics, Faculty of Science, Kasetsart University, Chatuchak, Bangkok, Thailand
[f] Division of Physics, School of Science, Walailak University, Nakhon Si Thammarat, Thailand
[g] Functional Materials and Nanotechnology Center of Excellence, Walailak University, Nakhon Si Thammarat, Thailand

Abstract

Combining various types of ferrites brings about magnetic properties desirable for different applications. This study aims to modify barium hexaferrite ($BaFe_{12}O_{19}$) by physically mixing it with cobalt ferrite ($CoFe_2O_4$). $BaFe_{12}O_{19}$/$CoFe_2O_4$ magnets were produced by ball-milling and pressing sol−gel-derived ferrite powders. The ferrite composites showed variations in magnetic properties from $BaFe_{12}O_{19}$ magnets with a saturation magnetization of 69.46 emu/g and a maximum energy product of 0.4529 MGOe. For the $BaFe_{12}O_{19}$:$CoFe_2O_4$ weight ratio of 4:1, both saturation and remanent magnetizations were increased due to the addition of $CoFe_2O_4$ with high magnetizations. However, the magnetizations were reduced when the $BaFe_{12}O_{19}$:$CoFe_2O_4$ ratio was reduced to 2:1. On the other hand, the coercivity was monotonously decreased with increasing $CoFe_2O_4$. Interestingly, the maximum energy product in this study was linearly decreased with the bulk density of the magnets from 3.59 to 3.15 g/cm^3. It is concluded that magnetic properties could be modified from a facile physical mixing of ferrites.

Keywords: Barium hexaferrite, Cobalt ferrite, Sol−gel reaction, Powder compaction, Nanocomposite magnet

1. Introduction

Nanostructured ferrites have a great range of applications in engineering and biomedicine. Renowned for their magnetic properties, ferrites at reduced dimensions also exhibit useful dielectric, photocatalytic, and antimicrobial properties. Such multifunctionality stems from different crystallographic structures and ion substitutions [1−5]. Among several types, barium hexaferrite ($BaFe_{12}O_{19}$) and strontium hexaferrite ($SrFe_{12}O_{19}$) have a hexagonal magnetoplumbite structure leading to a substantial crystalline anisotropy. These M-type hexaferrites exhibit high coercivity, providing a low-cost alternative to rare-earth permanent magnets [1,2]. In addition to a sizeable market share in permanent magnets, $BaFe_{12}O_{19}$ and $SrFe_{12}O_{19}$ have been implemented in data storage and microwave absorption [1,5]. On the other hand, spinel ferrites have a cubic structure resulting in lower coercivity. AFe_2O_4 (A^{2+} represents divalent cations) constitutes an important class of magnetic materials for sensors, high-frequency devices, photocatalyst, and data storage media [3,4]. To develop high-density perpendicular magnetic recording media, thin films of spinel cobalt ferrite ($CoFe_2O_4$) have been investigated [6,7].

Received 31 December 2022; revised 23 February 2023; accepted 27 February 2023.
Available online 14 April 2023

* Corresponding author at: Division of Physics, School of Science, Walailak University, Nakhon Si Thammarat, Thailand.
E-mail address: schitnar@mail.wu.ac.th (C. Sirisathitkul).

https://doi.org/10.33640/2405-609X.3292

Kneller and Hawig proposed in 1991 that combining hard and soft magnetic phases brings about an exchange-spring magnetic coupling in composites [8]. The hard/soft composite magnets exhibit high coercivity of the hard phase and high saturation magnetization of the soft phase. Hard/soft composite ferrites possess high electrical resistivity and chemical stability. However, particulate composites composed of hard and soft ferrite phases have a lower maximum energy product than that predicted by the micromagnetic simulation [9–15]. In some cases, large coercivity and magnetization are not simultaneously achieved. The saturation magnetization is usually increased at the expense of coercivity. Nevertheless, the properties of these composite ferrites can be tailored for other applications, including electromagnetic wave absorbers and high-frequency devices.

Besides individual ferrite characteristics and phase compositions, the properties of composite ferrites depend on the microstructure, which in turn is influenced by the synthesis and heat treatment processes. Soft ferrites were mostly incorporated into hard ferrites using the physical mixing and ball-milling of powders [9–12]. Ferrite powders can be synthesized via the sol–gel route, and composite ferrites may be obtained in one pot without subsequent mixing [13,14]. Moreover, Tavakolinia et al. increased the exchange coupling between $SrFe_{12}O_{19}$ and $Zn_{0.4}Co_{0.2}Ni_{0.4}Fe_2O_4$ prepared by the one-pot chemical synthesis [15].

$CoFe_2O_4$ is an interesting choice for producing composite ferrites because of its high saturation magnetization and large variation in coercivity. In addition to outstanding magnetic parameters, $CoFe_2O_4$ nanoparticles exhibit catalytic and antimicrobial properties, as reviewed by Mmelesi et al. [16]. Ion substitutions can tailor these properties in the sol–gel synthesis [17]. Furthermore, a large batch of $CoFe_2O_4$ nanoparticles can be synthesized from sol–gel reactions using environment-friendly chelating agents such as sago [18] and tapioca [19] starches. Incorporating $CoFe_2O_4$ through physical mixing [20], ball-milling [21], co-precipitation [22], or sol–gel synthesis [23], improves the magnetic and dielectric properties of $SrFe_{12}O_{19}$. For $BaFe_{12}O_{19}/CoFe_2O_4$ composites, the chemical co-precipitation has predominantly been used, and ball-milling is often employed to promote homogenization [24–26]. Other methods include the solid–state reaction [27] and the sol–gel route [28]. Interestingly, Davarpanah et al. also reported the antimicrobial activity of sol–gel-derived $BaFe_{12}O_{19}/CoFe_2O_4$ composites [28].

This study produces composite ferrites from sol–gel-derived $BaFe_{12}O_{19}$ and $CoFe_2O_4$ powders. Using the sol–gel route, high-purity ferrites can facilely be obtained at relatively low temperatures [29,30]. Importantly, the amounts of synthesized products are sufficient for powder compaction into bar magnets. The properties of magnets with the $BaFe_{12}O_{19}$:$CoFe_2O_4$ weight ratios of 2:1 and 4:1 are comparatively discussed.

2. Materials and methods

2.1. Fabrication of $BaFe_{12}O_{19}$ and $CoFe_2O_4$ powders

$BaFe_{12}O_{19}$ powders were synthesized by the sol–gel auto-combustion detailed in Ref. [31]. Raw materials were barium nitrate ($Ba(NO_3)_2$) (Himedia) and iron(III) nitrate nonahydrate ($Fe(NO_3)_3{\cdot}9H_2O$) (Sigma–Aldrich) with citric acid as a chelating agent. The synthesized products were calcined for 3 h at 1050 °C. $CoFe_2O_4$ powders were obtained from the sol–gel reaction between ($Co(NO_3)_2{\cdot}$ $6H_2O$) and iron(III) nitrate nonahydrate ($Fe(NO_3)_3{\cdot}9H_2O$), purchased from Sigma–Aldrich, with tapioca starch as a chelating agent described in Ref. [19]. The synthesized products in this study were calcined for a longer time of 10 h at a lower temperature of 600 °C. Ground $BaFe_{12}O_{19}$ and $CoFe_2O_4$ powders were simultaneously milled in a 3D ball mill (Nagao System) at 400 rpm for 10 min. The weight ratio of zirconia balls (10 mm in diameter) to powder was 5:1. The mixed powder obtained from the process in Fig. 1a was sieved through 100 mesh.

2.2. Preparation of magnets by powder compaction

Bar magnets were obtained from the powder compaction illustrated in Fig. 1b. To promote powder binding, 6 drops of 0.2 g polyvinylidene fluoride (PVDF) in 3 mL N-Methylpyrrolidone (NMP) were mixed with $BaFe_{12}O_{19}$ and $CoFe_2O_4$ powders. Each sample was then filled in a stainless mold cell with a 5 mm × 20 mm cross-section. An automatic hydraulic machine applied the pressure of 70 kg/cm^2 for 5 min. Bar magnets were obtained from the $BaFe_{12}O_{19}$:$CoFe_2O_4$ weight ratios of 2:1 (sample $2BaFe_{12}O_{19}/1CoFe_2O_4$) and 4:1 (sample $4BaFe_{12}O_{19}/1CoFe_2O_4$). In the case of higher $CoFe_2O_4$ compositions than sample $2BaFe_{12}O_{19}/1CoFe_2O_4$, bulk samples could not be formed under this compaction condition. Only loose powders were left, like $CoFe_2O_4$ powder compaction. After annealing at

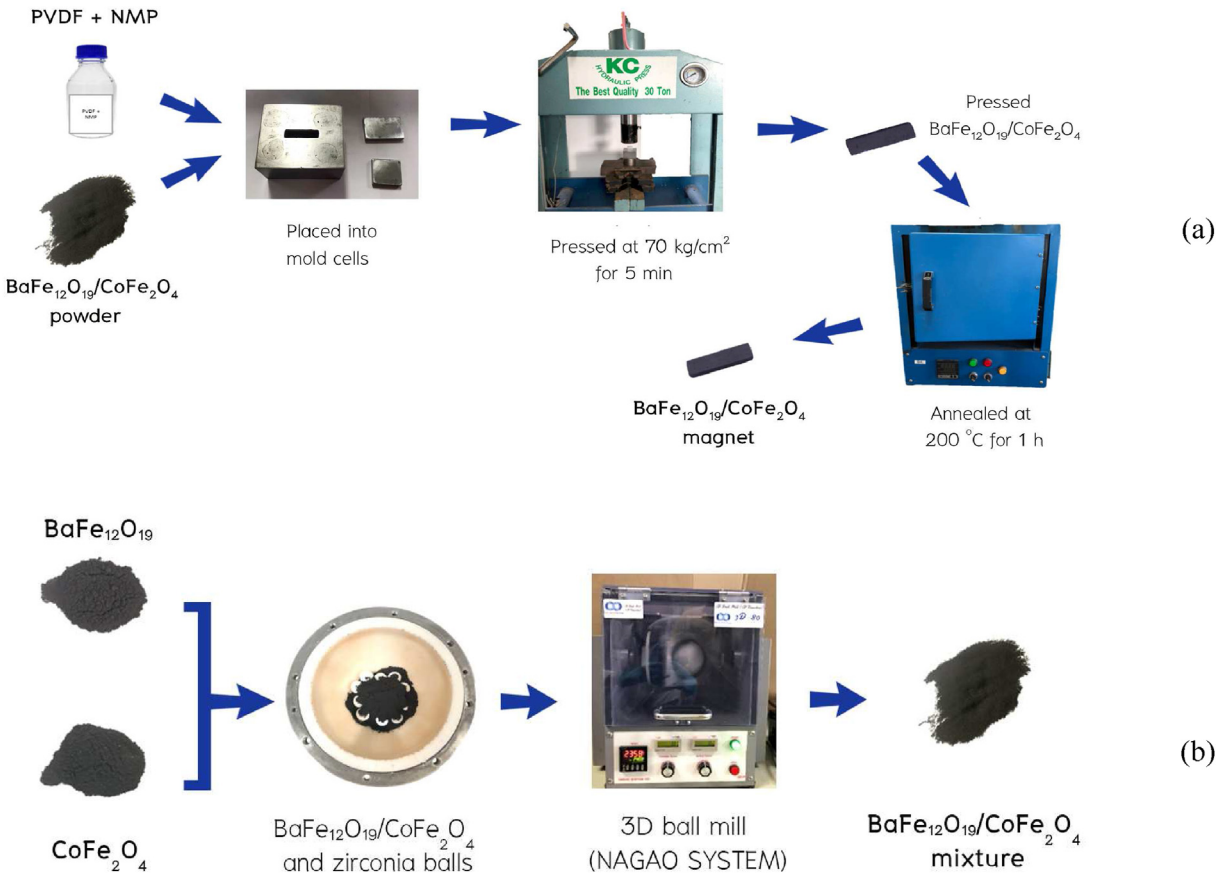

Fig. 1. Photographs from (a) ball-milling of $BaFe_{12}O_{19}$ and $CoFe_2O_4$ powders, and (b) powder compaction processes.

200 °C to eliminate residual PVDF and NMP for 1 h, each bar magnet was measured and weighted to determine its density. To compare with $BaFe_{12}O_{19}$ magnets, $BaFe_{12}O_{19}$ powders were exclusively pressed and referred to as sample $BaFe_{12}O_{19}$ magnet1. Without $CoFe_2O_4$, sample $BaFe_{12}O_{19}$ magnet2 was also prepared with the binders and annealed for 1 h at 200 °C.

2.3. Characterization of magnets

Phase structures of magnets were characterized by an X-ray diffractometer (XRD; Rigaku, SmartLab, Austin, TX, USA) using a CuKα_1 radiation (1.54060 Å). A scanning electron microscope (SEM; FEI, Quanta 250, Hillsboro, OR, USA) revealed the surface morphology of magnets. A vibrating sample magnetometer (VSM; in-house developed and calibrated with Lakeshore 730908) measured a mass magnetization (M) as a function of varying magnetic field (H) between −17.5 kOe and 17.5 kOe. The magnetic properties of each magnet were determined from resulting hysteresis loops as follows. The remanent magnetization (M_r) and the coercivity (H_c) were the y- and x-intercepts, respectively. The maximum energy product ($(BH)_{max}$) was calculated from the maximum area of rectangles fitted in the second quadrant. Because the magnetization is not saturated within the 17.5 kOe field, the saturation magnetization (M_s) was estimated from the plot between M and $1/H^2$. Using the law of approach to saturation in a regime close to the maximum applied field with b as a constant;

$$M = M_s\left[1 - \frac{b}{H^2}\right] \quad (1)$$

3. Results and discussion

In Fig. 2, the sol–gel-derived powders exhibit XRD patterns consistent with the standards of single-phase ferrites. The face-centered cubic $CoFe_2O_4$ phase (JCPDS: 01-080-6487) is indexed by the diffraction from the (220), (311), (222), (400), (422), (511), and (440) crystallographic planes at 30.23°, 35.61°, 37.25°, 43.28°, 53.70°, 57.25°, and 62.87°, respectively. For the hexagonal close packed $BaFe_{12}O_{19}$ (JCPDS: 00-043-0002), the peaks at 30.31°,

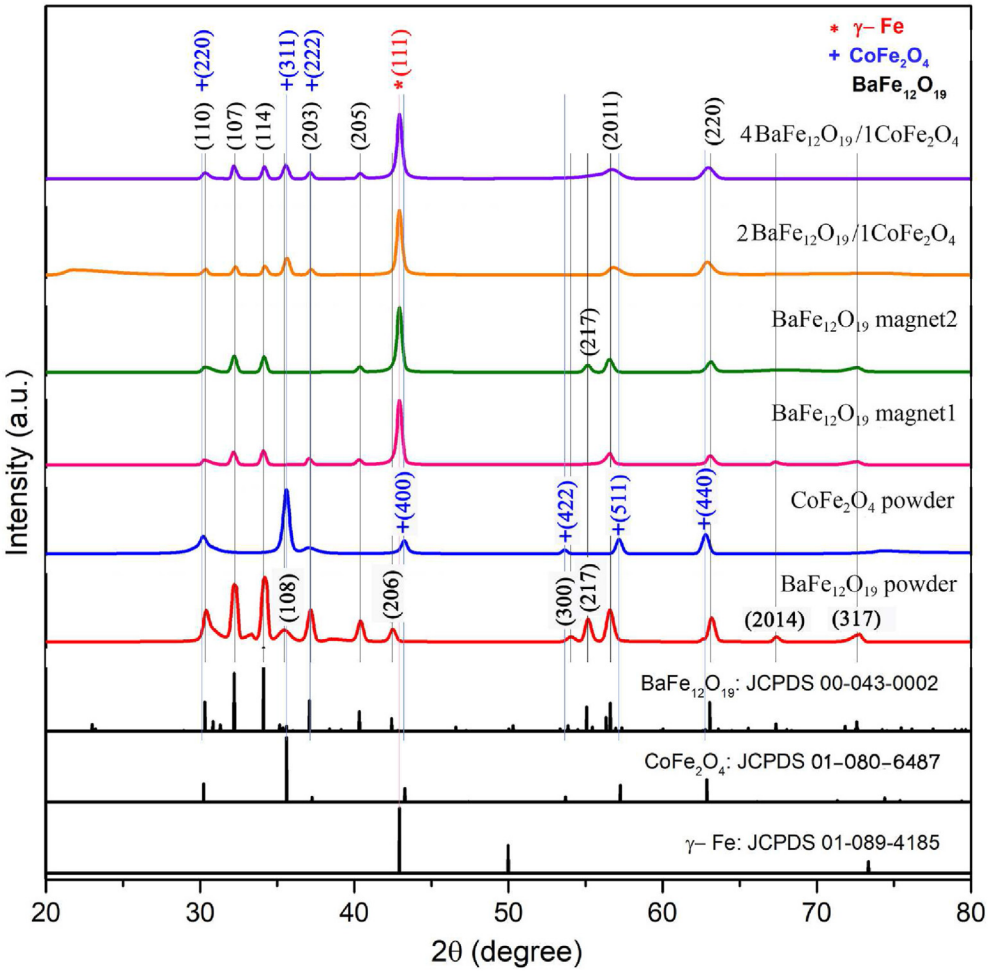

Fig. 2. XRD spectra of $BaFe_{12}O_{19}/CoFe_2O_4$ magnets compared to $BaFe_{12}O_{19}$ from powder compaction, $BaFe_{12}O_{19}$ and $CoFe_2O_4$ powders.

32.20°, 34.11°, 35.60°, 37.08°, 40.32°, 42.42°, 53.86°, 55.06°, 56.60°, 63.06°, 67.36°, and 72.59° correspond to the (110), (107), (114), (108), (203), (205), (206), (300), (217), (2011), (220), (2014), and (317) planes, respectively.

When $BaFe_{12}O_{19}$ powders are consolidated into magnets, the XRD patterns drastically change. The peak with the highest intensity, around 43° is in the vicinity of the minor $BaFe_{12}O_{19}$ peak but closer to the major peak from the (111) plane of γ-Fe (JCPDS: 01-089-4185). This presence of secondary iron phase in both $BaFe_{12}O_{19}$ magnet1 and $BaFe_{12}O_{19}$ magnet2 indicates that PVDF and NMP in the powder compaction do not influence this phase formation. Only two minor $BaFe_{12}O_{19}$ peaks from magnets pressed with and without the binders are different.

The XRD spectra of $BaFe_{12}O_{19}/CoFe_2O_4$ magnets resemble those of $BaFe_{12}O_{19}$ magnets because of their higher $BaFe_{12}O_{19}$ compositions. In addition, the $CoFe_2O_4$ peaks from the (220), (311), and (222) planes are observed. The γ-Fe phase also exists in ferrite composites. Because Fig. 2 confirms the single-phase ferrite in each starting powder, the Fe phase formation is attributed to applied pressure and temperature in the preparation of magnets.

Calcination temperature is a critical factor in crystallizing ferrite phases. For $BaFe_{12}O_{19}$, the phase diagram of the Fe_2O_3–BaO system suggests the calcination temperature above 800 °C for 15 mol% BaO [32]. The experimental results by Hoque et al. revealed that the $BaFe_{12}O_{19}$ and $CoFe_2O_4$ phases in composites were crystallized at 800 °C [24]. However, a homogeneous single-phase $BaFe_{12}O_{19}$ was only obtained by calcining at 1000–1100 °C. This finding, consistent with other reports on enhancing $BaFe_{12}O_{19}$ impurity and particle size at higher calcination temperatures [33,34], is confirmed in this study.

The SEM micrograph of $CoFe_2O_4$ in Fig. 3a shows some microclusters among nanoparticles. Smaller particles are advantageous because two phases should be in close contact to promote the exchange-spring magnetic coupling in composites [12]. Larger clusters with a flat surface are observed in $BaFe_{12}O_{19}$

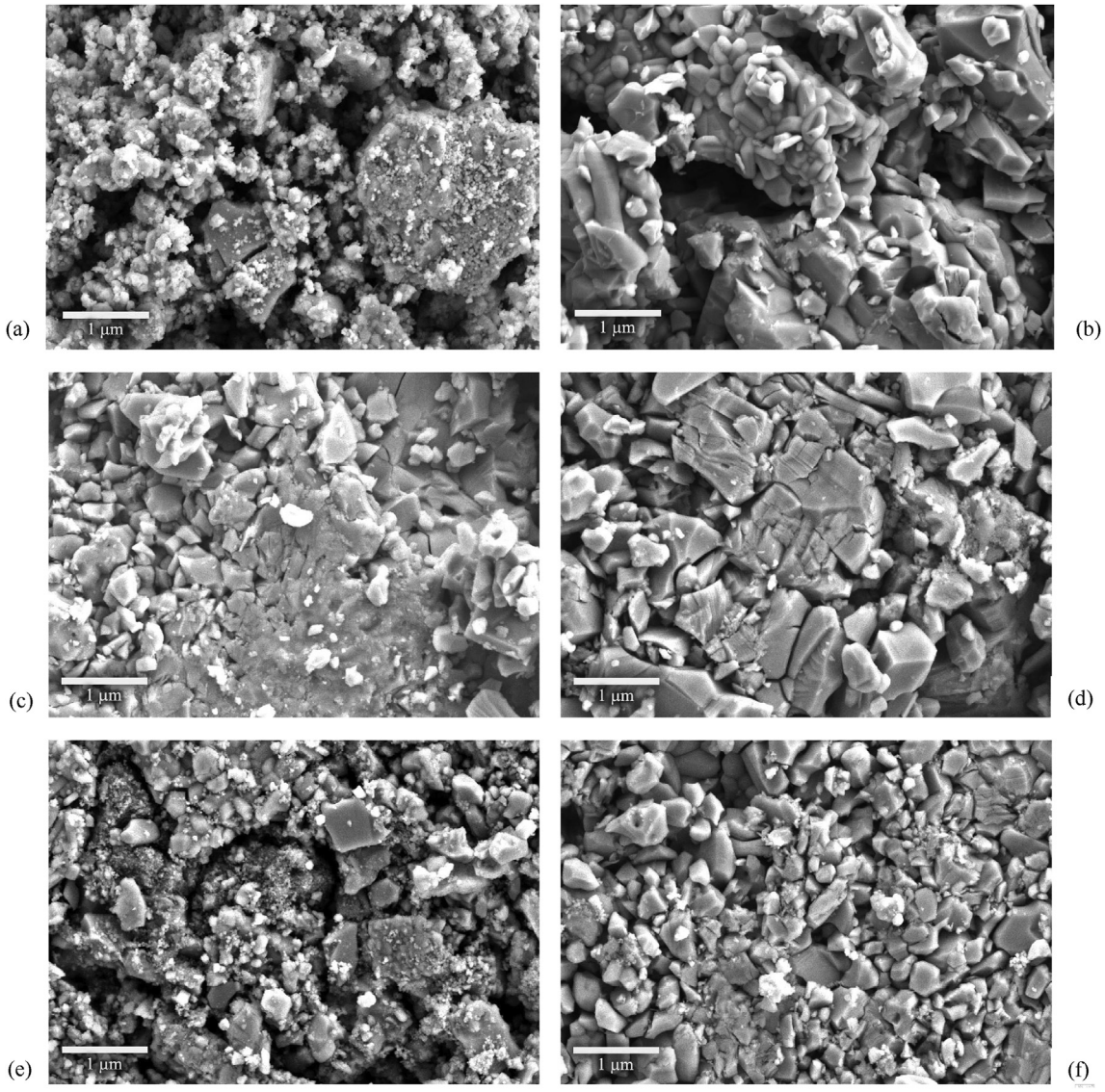

Fig. 3. FESEM micrographs of samples; (a) $CoFe_2O_4$ powders, (b) $BaFe_{12}O_{19}$ powders, (c) $BaFe_{12}O_{19}$ magnet1, (d) $BaFe_{12}O_{19}$ magnet2, (e) $2BaFe_{12}O_{19}/1CoFe_2O_4$ and (f) $4BaFe_{12}O_{19}/1CoFe_2O_4$ magnets.

in Fig. 3b. Agglomeration due to van der Waals forces is also prominent in $SrFe_{12}O_{19}$ [11]. The voids between these clusters are filled with particles of the order of 100 nm. The effect of powder compaction is shown in Fig. 3c and d. Clusters in magnets are merged or brought in contact. Whereas the effect of ball-milling on the XRD peak broadening is not observed in Fig. 2, the SEM micrographs of $BaFe_{12}O_{19}/CoFe_2O_4$ magnets in Fig. 3e and f reveal particles of the order of 100 nm without micro-clusters because of the ball-milling. These particles are packed among nanoparticles previously identified as the $CoFe_2O_4$ phase. More nanoparticles in Fig. 3e are consistent with the $CoFe_2O_4$ increase in the sample $2BaFe_{12}O_{19}/1CoFe_2O_4$.

In Fig. 4a, the hysteresis loop of $CoFe_2O_4$ powders is distinguished for its high magnetization. The remanent and saturation magnetizations listed in Table 1 are 33.32 and 71.22 emu/g, respectively. The previously reported saturation magnetization of $CoFe_2O_4$ is as high as 80 emu/g [35]. On the other hand, $BaFe_{12}O_{19}$ powders exhibit lower magnetizations and a wide hysteresis loop, characteristics of hard magnetic materials. The coercivity of $BaFe_{12}O_{19}$ powders (2,137.58 Oe) is substantially larger than that of $CoFe_2O_4$ (1,692.29 Oe). This coercivity of $BaFe_{12}O_{19}$ is still much lower than those previously used in producing $BaFe_{12}O_{19}/CoFe_2O_4$ composites [24,25], whereas the saturation magnetization of 65.19 emu/g is comparable.

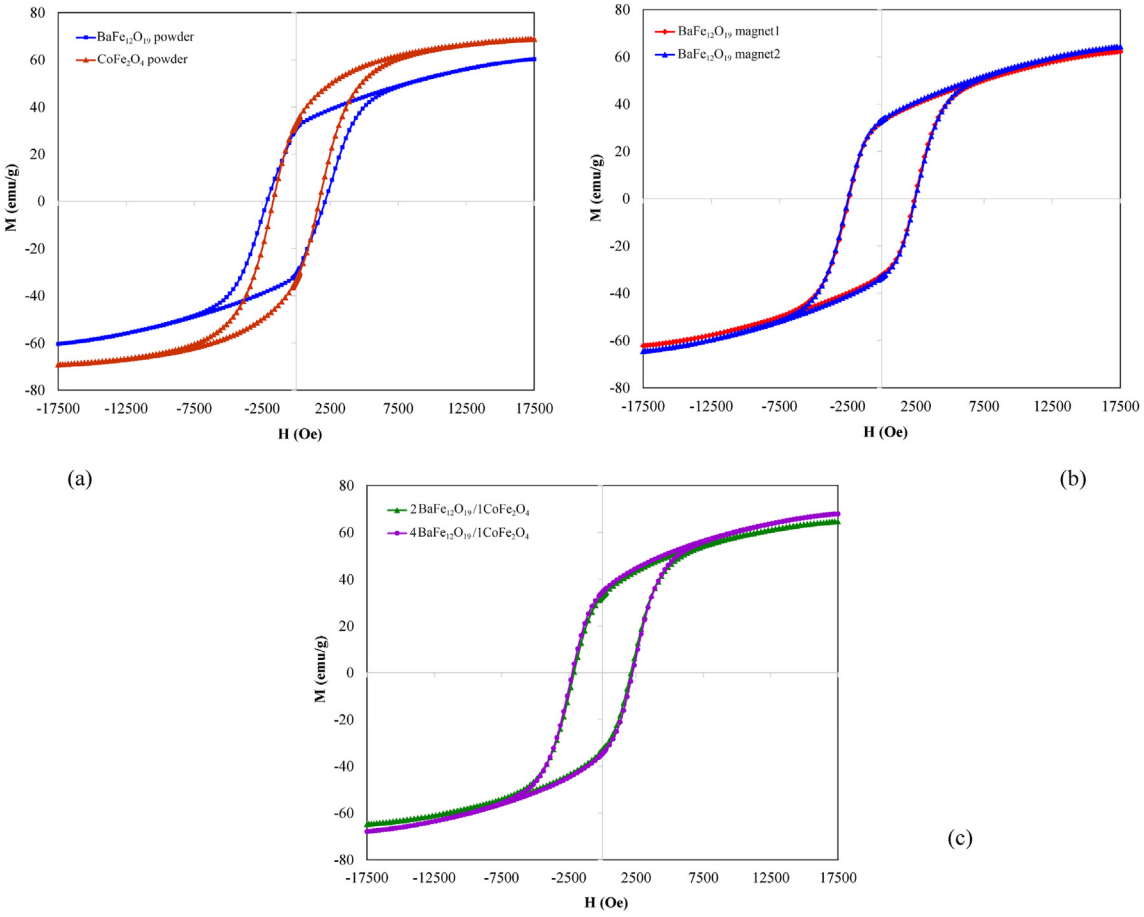

Fig. 4. Hysteresis loops of (a) $BaFe_{12}O_{19}$ and $CoFe_2O_4$ powders, (b) $BaFe_{12}O_{19}$ magnets, and (c) $BaFe_{12}O_{19}/CoFe_2O_4$ magnets.

After the powder compaction, the hysteresis loops of $BaFe_{12}O_{19}$ magnets in Fig. 4b are modified with higher coercivity and magnetizations. The Fe phase formation in the compaction shown by XRD does not have an adverse effect on the magnetic properties. As compared in Table 1, higher coercivity (2,467 Oe), remanent magnetization (33.20 emu/g), and saturation magnetization (69.46 emu/g) are obtained with the binder addition ($BaFe_{12}O_{19}$ magnet2). The influence of the binders in the powder compaction is related to the density. Adding binders reduces the porosity leading to a higher density of 3.59 g/cm^3. In addition to higher magnetization, the coercivity is increased due to enhanced magnetic interaction between densely packed $BaFe_{12}O_{19}$ particles. The increases in magnetization and coercivity after consolidating $BaFe_{12}O_{19}$ powders were also reported by Timofeev et al. [36].

The $CoFe_2O_4$ addition decreases the total density of the magnets to 3.47 and 3.15 g/cm^3 when the $BaFe_{12}O_{19}$:$CoFe_2O_4$ ratio is 4:1 and 2:1, respectively.

Table 1. Density and magnetic properties of $BaFe_{12}O_{19}/CoFe_2O_4$ magnets compared to $BaFe_{12}O_{19}$ magnets as well as $BaFe_{12}O_{19}$ and $CoFe_2O_4$ powders.

Sample	Density (g/cm^3)	Magnetic properties				
		H_c (Oe)	M_r (emu/g)	M_s (emu/g)	M_r/M_s	$(BH)_{max}$ (MGOe)
$CoFe_2O_4$ powder	–	1,692.29 ± 0.02	33.32 ± 0.046	71.22 ± 0.20	0.468	–
$BaFe_{12}O_{19}$ powder	–	2,137.58 ± 0.20	31.15 ± 0.16	65.19 ± 0.13	0.478	–
$BaFe_{12}O_{19}$ magnet1	3.25	2,404.86 ± 3.32	32.44 ± 0.01	66.79 ± 0.20	0.486	0.3633
$BaFe_{12}O_{19}$ magnet2	3.59	2,467.17 ± 1.02	33.20 ± 0.03	69.46 ± 0.13	0.478	0.4529
$2BaFe_{12}O_{19}/1CoFe_2O_4$	3.15	2,112.99 ± 0.14	32.90 ± 0.04	68.42 ± 0.08	0.481	0.3238
$4BaFe_{12}O_{19}/1CoFe_2O_4$	3.47	2,241.79 ± 0.14	34.65 ± 0.01	72.52 ± 0.01	0.478	0.4329

These densities fall into the 3.0–4.1 g/cm^3 range previously reported in $BaFe_{12}O_{19}/CoFe_2O_4$ composites from the co-precipitation [25]. In Fig. 4c, $BaFe_{12}O_{19}/CoFe_2O_4$ magnets exhibit smooth hysteresis loops from a single magnetization reversal process, indicating the magnetic coupling between $BaFe_{12}O_{19}$ and $CoFe_2O_4$ phases [20,23]. However, the M_r/M_s ratios in Table 1 around 0.48 suggest that the coupling is weak. The comparable values were previously reported [21,23], but the M_r/M_s ratio larger than 0.5 could also be obtained in $SrFe_{12}O_{19}/CoFe_2O_4$ composites [22].

The coercivity is reduced to below 2,400 Oe with increasing $CoFe_2O_4$ due to intervening $CoFe_2O_4$ particles among $BaFe_{12}O_{19}$. Notably, a higher $BaFe_{12}O_{19}$:$CoFe_2O_4$ ratio of 4:1 increases the magnetizations. Compared to the sample $BaFe_{12}O_{19}$ magnet2, both remanent and saturation magnetizations are increased by adding $CoFe_2O_4$ with a high magnetization. The saturation magnetization is higher than overall reports in $BaFe_{12}O_{19}/CoFe_2O_4$ composites [24–28]. However, a lower coercivity attributed to larger $BaFe_{12}O_{19}$ particles than those in the previous reports [24,25], results in the maximum energy product of only 0.4329 MGOe. For the $BaFe_{12}O_{19}$:$CoFe_2O_4$ ratio of 2:1, the value is further reduced to 0.3238 MGOe because increasing $CoFe_2O_4$ lower both coercivity and remanent magnetization.

Like multiferroic systems [37], the properties of magnetic composites are regulated by the interface between the compositional phases. The exchange-spring magnetic coupling is sensitive to the grain boundaries and the ratio of soft magnetic grain size to hard magnetic domain wall width [24]. For ferrite composites, the variations in anisotropy and exchange stiffness at the interface are less marked than those in metallic composite magnets. Also, the grain size of smaller $CoFe_2O_4$ particles in Fig. 3a are in the same order of the $BaFe_{12}O_{19}$ domain wall width to promote magnetic coupling [24]. However, enhancing the exchange-spring magnetic coupling between ferrite particles is challenging because the interface is not as clearly defined and controlled as in layered structures [8,24]. Increasing the maximum energy product in particulate composites to meet the requirement for the application as permanent magnets remains elusive.

Although the exchange-spring magnetic coupling across the interface cannot be analyzed in this study, the results in Table 1 show that magnetic properties of $BaFe_{12}O_{19}$ can be regulated with parameters in fabrication. The coercivity is monotonously decreased with the $CoFe_2O_4$ addition. Interestingly, the plot in Fig. 5 exhibits a linear reduction in the maximum energy product with the bulk density of magnets from 3.15 to 3.59 g/cm^3 in this study.

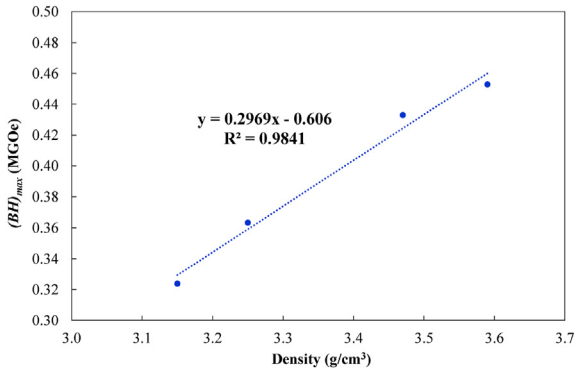

Fig. 5. Plot of the maximum energy product against the bulk density of $BaFe_{12}O_{19}$ and $BaFe_{12}O_{19}/CoFe_2O_4$ magnets.

4. Conclusions

The coercivity and magnetization of $BaFe_{12}O_{19}$ magnets are modified by ball-milling and pressing with sol–gel-derived $CoFe_2O_4$. Because the $CoFe_2O_4$ has higher magnetizations than $BaFe_{12}O_{19}$, the $BaFe_{12}O_{19}/CoFe_2O_4$ magnets with the ratio of 4:1 exhibit higher remanent and saturation magnetizations than those of $BaFe_{12}O_{19}$. However, adding $CoFe_2O_4$ reduces the coercivity of $BaFe_{12}O_{19}$, and the maximum energy product $BaFe_{12}O_{19}/CoFe_2O_4$ magnets (0.4329 MGOe) is slightly less than that of the $BaFe_{12}O_{19}$ magnet (0.4529 MGOe). For the $BaFe_{12}O_{19}/CoFe_2O_4$ magnets with a ratio of 2:1, both coercivity and remanent magnetization are decreased, reducing the maximum energy product to only 0.3238 MGOe. The maximum energy product of $BaFe_{12}O_{19}$ and $BaFe_{12}O_{19}/CoFe_2O_4$ magnets in this study is linearly decreased with the reduction in the bulk density from 3.15 to 3.59 g/cm^3.

Conflict of interest

The authors declare no conflict of interest.

Acknowledgments

This work is funded by Thailand Center of Excellence in Physics (ThEP-63-PIP-WU3). The authors acknowledge facility support by Dr. Chesta Ruttanapun of King Mongkut's Institute of Technology Ladkrabang.

References

[1] R. Pullar, Hexagonal ferrites: a review of the synthesis, properties and applications of hexaferrite ceramics, Prog. Mater. Sci. 57 (2012) 1191–1334.

[2] C. de Julián Fernández, C. Sangregorio, J. de la Figuera, B. Belec, D. Makovec, A. Quesada, Progress and prospects of hard hexaferrites for permanent magnet applications, J. Phys. D: Appl. Phys. 54 (2021) 153001.
[3] T.N. Pham, T.Q. Huy, A.-T. Le, Spinel ferrite (AFe_2O_4)-based heterostructured designs for lithium-ion battery, environmental monitoring, and biomedical applications, RSC Adv. 10 (2020) 31622.
[4] S.K. Dutta, M. Akhter, J. Ahmed, Md.K. Amin, P.K. Dhar, Synthesis and catalytic activity of spinel ferrites: a brief review, Biointerf. Res. Appl. Chem. 12 (2022) 4399–4416.
[5] S.E. Shirsath, R.H. Kadam, K.M. Batoo, D. Wang, S. Li, Co–Al-substituted strontium hexaferrite for rare earth free permanent magnet and microwave absorber application, J. Phys. D: Appl. Phys. 54 (2021) 024001.
[6] S.E. Shirsath, X. Liu, Y. Yasukawa, S. Li, A. Morisako, Switching of magnetic easy-axis using crystal orientation for large perpendicular coercivity in $CoFe_2O_4$ thin film, Sci. Rep. 6 (2016) 30074.
[7] S.E. Shirsath, D. Wang, J. Zhang, A. Morisako, S. Li, X. Liu, Single-crystal-like textured growth of $CoFe_2O_4$ thin film on an amorphous substrate: a self-bilayer approach, ACS Appl. Electron. Mater. 2 (2020) 3650–3657.
[8] E.F. Kneller, R. Hawig, The exchange-spring magnet: a new material principle for permanent magnets, IEEE Trans. Magn. 27 (1991) 3588–3600.
[9] S.G. Greculeasa, C. Comanescu, N. Iacob, A. Kuncser, Exchange coupled nanocomposites: magnetoplumbite Sr ferrite and magnetite, Rom. J. Phys. 67 (2022) 606.
[10] S.A. Sam, A.P. Balan, A. Kaipamangalath, M.R. Varma, R.R. Nair, S. Thomas, Nanocomposite permanent magnets based on $SrFe_{12}O_{19}$-Fe_3O_4, J. Supercond. Nov. Magn. 34 (2021) 3333–3344.
[11] J. Xia, X. Wu, Y. Huang, W. Wu, J. Liang, Q. Li, Enhancements of saturation magnetization and coercivity in $Ni_{0.5}Zn_{0.5}Fe_2O_4/SrFe_{12}O_{19}$ composite powders by exchange-coupling mechanism, J. Mater. Sci: Mater. Electron. 30 (2019) 11682–11693.
[12] P. Jenuš, A. Ucakar, S. Repše, C. Sangregorio, M. Petrecca, M. Albino, R. Cabassi, C. de Julian Fernandez, B. Belec, Magnetic performance of $SrFe_{12}O_{19}$-$Zn_{0.2}Fe_{2.8}O_4$ hybrid magnets prepared by spark plasma sintering, J. Phys. D: Appl. Phys. 54 (2021) 204002.
[13] M.K. Manglam, S. Kumari, J. Mallick, A. Shukla, M. Kar, Magnetic interaction between soft and hard ferrimagnetic phases in $BaFe_{12}O_{19} + CuFe_2O_4$ composite, Phys. Scripta 560 (2022) 169569.
[14] N.A. Algarou, Y. Slimani, M.A. Almessiere, F.S. Alahmari, M.G. Vakhitov, D.S. Klygach, S.V. Trukhanov, A.V. Trukhanov, A. Baykal, Magnetic and microwave properties of $SrFe_{12}O_{19}/MCe_{0.04}Fe_{1.96}O_4$ (M = Cu, Ni, Mn, Co and Zn) hard/soft nanocomposites, J. Mater. Res. Technol. 9 (2020) 5858–5870.
[15] F. Tavakolinia, M. Yousefi, S.S.S. Afghahi, S. Baghshahi, S. Samadi, Synthesis of novel hard/soft ferrite composites particles with improved magnetic properties and exchange coupling, Proc. Appl. Ceram. 12 (2018) 248–256.
[16] O.K. Mmelesi, N. Masunga, A. Kuvarega, T.T. Nkambule, B.B. Mamba, K.K. Kefeni, Cobalt ferrite nanoparticles and nano-composites: photocatalytic, antimicrobial activity and toxicity in water treatment, Mater. Sci. Semicond. Proc. 123 (2021) 105523.
[17] K.S. Lohar, A.M. Pachpinde, M.M. Langade, R.H. Kadam, S.E. Shirsath, Self-propagating high temperature synthesis, structural morphology and magnetic interactions in rare earth Ho^{3+} doped $CoFe_2O_4$ nanoparticles, J. Alloys Compd. 604 (2014) 204–210.
[18] A. Hunyek, C. Sirisathitkul, C. Mahaphap, U. Boonyang, W. Tangwatanakul, Sago starch: chelating agent in sol–gel synthesis of cobalt ferrite nanoparticles, J. Aust. Ceram. Soc. 53 (2017) 173–176.
[19] A. Hunyek, C. Sirisathitkul, K. Koyvanich, Tapioca starch in the sol–gel synthesis of cobalt ferrites with divalent cation substitutions, Karbala Int. J. Mod. Sci. 8 (2022) 10.
[20] D. Roy, P.S. Anil Kumar, Exchange spring behaviour in $SrFe_{12}O_{19}$-$CoFe_2O_4$ nanocomposites, AIP Adv. 5 (2015) 077137.
[21] V. Bilovol, M. Sikora, A. Szkudlarek, M. Gajewska, Magnetic interactions in $SrFe_{12}O_{19}/CoFe_2O_4$ composite: influence of ball milling frequency and annealing temperature, J. Magn. Magn. Mater. 564 (2022) 170217.
[22] K. Dhabekar, K.M. Kant, Magnetic and dielectric response of $CoFe_2O_4$-$SrFe_{12}O_{19}$ nanocomposites, J. Supercond. Nov. Magn. 34 (2021) 907–912.
[23] P. Maltoni, T. Sarkar, G. Barucca, G. Varvaro, F. Locardi, D. Peddis, R. Mathieu, Tuning the magnetic properties of hard–soft $SrFe_{12}O_{19}/CoFe_2O_4$ nanostructures via composition/interphase coupling, J. Phys. Chem. C 125 (2021) 5927–5936.
[24] S.M. Hoque, C. Srivastava, V. Kumar, N. Venkatesh, H.N. Das, D.K. Saha, K. Chattopadhyay, Exchange-spring mechanism of soft and hard ferrite nanocomposites, Mater. Res. Bull. 48 (2013) 2871–2877.
[25] K. Polley, T. Alam, J. Bera, Synthesis and characterization of $BaFe_{12}O_{19}$-$CoFe_2O_4$ ferrite composite for high-frequency antenna application, J. Aust. Ceram. Soc. 56 (2020) 1179–1186.
[26] L. Rifai, F. Fattouh, K. Habanjar, N. Yaacoub, R. Awad, Exchange spring behaviour in $BaFe_{12}O_{19}/CoFe_2O_4$ magnetic nanocomposites, J. Alloys Compd. 868 (2021) 159072.
[27] N. Hooda, R. Sharma, A. Hooda, S. Khasa, Structural refinement, dielectric and spin exchange magnetic analysis of (1-x)$BaFe_{12}O_{19}$-(x)$CoFe_2O_4$ composites, Phys. B: Cond. Matter 643 (2022) 414191.
[28] A.M. Davarpanah, A. Rahdar, M.A. Dastnae, O. Zeybek, H. Beyzaei, (1-x)$BaFe_{12}O_{19}$/x$CoFe_2O_4$ hard/soft magnetic nano-composites: synthesis, physical characterization, and antibacterial activities study, J. Mol. Struct. 1175 (2019) 445–449.
[29] S.E. Shirsath, S.S. Jadhav, M.L. Mane, S. Li, Ferrites obtained by sol–gel method, in: L. Klein, M. Aparicio, A. Jitianu, eds., Handbook of Sol–Gel Science and Technology, second ed., Springer International. 2016, pp. 695–735.
[30] A. Hunyek, C. Sirisathitkul, P. Harding, Synthesis and characterization of $CoFe_2O_4$ particle by PVA sol–gel method, Adv. Mater. Res. 93 (2010) 659–663.
[31] T. Charoensuk, W. Thongsamrit, C. Ruttanapun, P. Jantaratana, C. Sirisathitkul, Loading effect of sol–gel derived barium hexaferrite on magnetic polymer composites, Nanomaterials 11 (2021) 558.
[32] W. Martienssen, H. Warlimont, Springer Handbook of Condensed Matter and Materials Data, Springer. 2005.
[33] M. Rianna, T. Sembiring, M. Situmorang, C. Kurniawan, A.P. Tetuko, E.A. Setiadi, I. Priyadi, M. Ginting, P. Sebayang, Effect of calcination temperature on microstructures, magnetic properties, and microwave absorption on $BaFe_{11.6}Mg_{0.2}Al_{0.2}O_{19}$ synthesized from natural iron sand, Case Stud. Therm. Eng. 13 (2019) 100393.
[34] C. Granados-Miralles, P. Jenuš, On the potential of hard ferrite ceramics for permanent magnet technology: a review on sintering strategies, J. Phys. D: Appl. Phys. 54 (2021) 303001.
[35] M. Grigorova, H.J. Blythe, V. Blaskov, V. Rusanov, V. Petkov, V. Masheva, D. Nihtianova, Ll.M. Martinez, J.S. Muñoz, M. Mikhov, Magnetic properties and Mössbauer spectra of nanosized $CoFe_2O_4$ powders, J. Magn. Magn. Mater. 183 (1998) 163–172.
[36] A.V. Timofeev, V.G. Kostishin, D.B. Makeev, D.N. Chitanov, Magnetic properties of barium hexaferrite compacted nanopowders, Tech. Phys. 64 (2019) 1484–1487.
[37] S.E. Shirsath, M. Hussein N. Assadi, J. Zhang, N. Kumar, A.S. Gaikwad, J. Yang, H.E. Maynard-Casely, Y.Y. Tay, J. Du, H. Wang, Y. Yao, Z. Chen, J. Zhang, S. Zhang, S. Li, D. Wang, Interface-driven multiferroicity in cubic $BaTiO_3$-$SrTiO_3$ nanocomposites, ACS Nano 16 (2022) 15413–15424.